

# Learning Agile Skills via Adversarial Imitation of Rough Partial Demonstrations

Chenhao Li<sup>1,2</sup>, Marin Vlastelica<sup>1</sup>, Sebastian Blaes<sup>1</sup>, Jonas Frey<sup>2,1</sup>,  
Felix Grimminger<sup>1</sup>, Georg Martius<sup>1</sup>

<sup>1</sup>Max Planck Institute for Intelligent Systems, Germany

<sup>2</sup>Robotic Systems Lab, ETH Zurich, Switzerland  
chenhao.li@tuebingen.mpg.de

**Abstract:** Learning agile skills is one of the main challenges in robotics. To this end, reinforcement learning approaches have achieved impressive results. These methods require explicit task information in terms of a reward function or an expert that can be queried in simulation to provide a target control output, which limits their applicability. In this work, we propose a generative adversarial method for inferring reward functions from partial and potentially physically incompatible demonstrations for successful skill acquisition where reference or expert demonstrations are not easily accessible. Moreover, we show that by using a Wasserstein GAN formulation and transitions from demonstrations with rough and partial information as input, we are able to extract policies that are robust and capable of imitating demonstrated behaviors. Finally, the obtained skills such as a backflip are tested on an agile quadruped robot called Solo 8 and present faithful replication of hand-held human demonstrations.

**Keywords:** Adversarial, Imitation Learning, Legged Robots

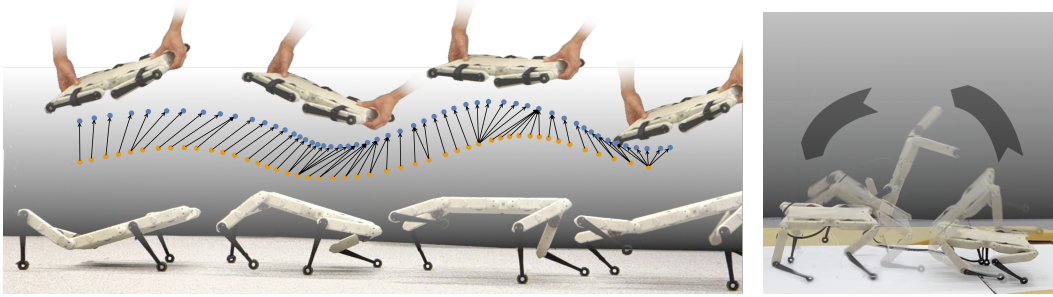


Figure 1: Examples of how our method (WASABI) uses rough demonstrations via hand-held robot-base motion to achieve agile physical behaviors. The illustrated performance measure is the Dynamic Time Warping distance of the base trajectories (left). We also learn a backflip behavior (right).

## 1 Introduction

Obtaining dynamic skills for autonomous machines has been a cardinal challenge in robotics. In the field of legged systems, many attempts have been made to attain diverse skills using conventional inverse kinematics techniques [1, 2]. In recent years, learning-based quadrupedal locomotion has been achieved by reinforcement learning (RL) approaches to address more complex environments and improve performance [3, 4, 5, 6]. However, the demand for acquiring more dynamic motions has brought new challenges to robot learning. A primary shortage of motivating desired behaviors by reward engineering is the arduous reward-shaping process involved. It can sometimes become extremely demanding in developing highly dynamic skills such as jumping and backflipping, where various terms of motivation and regularization require elaborated refinement.

Given the availability of some expert references, one possible solution is Imitation Learning (IL), which aims to mimic expert behaviors in a given task. In this framework, the agent is trained to perform a task from demonstrations by learning a mapping between observations and actions with either offline (e.g. behavioral cloning [7, 8]) or interactive (e.g. DAgger, SMILe [9]) methods. Generic IL methods could potentially reduce the problem of teaching a task to that of providing demonstrations, without the need for explicit programming or designing reward functions specific to the task [10]. Another related approach to replicating exerted motions of an expert is Inverse Reinforcement Learning (IRL). In IRL, the expert reward function is inferred given its policy or observed behaviors [11, 12, 13]. IRL is in general computationally expensive, and efforts are required to deal with ambiguous reward functions without making strong assumptions [14].

More recently, Generative Adversarial Imitation Learning (GAIL)[15] draws a connection between imitation learning and generative adversarial networks (GANs) [16], which train a generative model (generator) by having it confuse a discriminative classifier (discriminator). The task of the discriminator is to distinguish between data generated by the generator and the true data distribution. In the setting of GAIL, the true data distribution is the expert state-action distribution, while the learned policy is treated as the generator. The output of the discriminator can then be used as a reward that encourages the learning agent to generate similar behaviors to the demonstration. Analogously, the technique has been used for learning adversarial motion priors (AMP) [17], where the output of the discriminator is used as an additional style reward to the actual task reward, that is available beforehand. In a sense, AMP enables solving well-defined tasks in a specific style specified by a reference motion, without requiring access to underlying expert actions.

In this work, we present a novel adversarial imitation learning method named Wasserstein Adversarial Behavior Imitation (WASABI). We show that we are able to extract sensible task rewards from rough and partial demonstrations by utilizing adversarial training for obtaining agile skills in a sim-to-real setting. In contrast to Peng et al. [17], our approach does not require any prior information about the task at hand in form of a specific reward function, but only reasonable task-agnostic regularization terms in addition to the adversarial reward that make the robot motion more stable. Most importantly, we achieve this without having access to samples from an expert policy, but rather hand-held human demonstrations that are physically incompatible to the robot itself. To the best of our knowledge, this is the first time that highly dynamic skills are obtained from limited reference information. In summary, our contributions include: (i) An adversarial approach for learning from partial, physically incompatible demonstrations. (ii) Analysis of the Least-Squares vs. Wasserstein GAN loss for reward inference. (iii) Experimental validation in simulation and on a quadruped robot. Supplementary videos for this work are available at <https://sites.google.com/view/corl2022-wasabi/home>.

## 2 Related Work

Advances in robotics and communication technologies have spawned many potential applications that require intelligent systems to be able to not only make decisions but also to perform physical movements in an expected manner. However, in many cases, the desired behavior may not be discovered by a learning agent due to sub-optimal parameter settings or algorithmic limitations [18, 19]. While learning a task might be stated as an optimization problem, it has become widely accepted that having prior knowledge provided by an expert is more effective and efficient than attempting to solve the problem from scratch [20, 21].

The idea of imitation learning has been formed decades ago, raising solutions in conceptual and computational models to replicate motions from demonstrations [22, 23, 24]. It has been commonly acknowledged that imitating learning entails three major approaches: model-based imitation learning, learning a control policy directly, and learning from demonstrated trajectories. In the first approach, algorithms are applied to learn the parameters of the dynamics model to ensure that all executed motions closely follow the demonstration [25, 26, 27]. In the second approach, also known as behavioral cloning, the agent tries to reproduce the observed state-action pairs of the expert policy [7, 8]. Behavioral cloning often faces the problems of error compounding and poor generalization, which can lead to unstable policy output, particularly in out-of-distribution regions [28]. Alternatively, reference motions can be learned using an imitation goal, which is often implemented as a tracking objective that aims to reduce the pose error between the simulated character and target poses from a reference motion [29, 30, 31, 32]. A common strategy to estimate the pose error is to use a phase

variable as an additional input to the controller to synchronize the agent with a specific reference motion [33, 32, 34]. This method typically works well for replicating single motion clips, but it may fail to scale to datasets with multiple reference motions which may not be synchronized and aligned according to a single-phase variable [17].

Instead of employing a handcrafted imitation objective, adversarial IL techniques train an adversarial discriminator to distinguish between behaviors generated by an agent and demonstrations [14, 15]. While these methods have shown some promise for motion imitation tasks [35, 36], adversarial learning algorithms are notoriously unstable, and the resulting motion quality still lags well behind that of state-of-the-art tracking-based systems. Especially in the low-data regime, adversarial models can take a long time to converge [37, 17]. In some cases, adversarial IL techniques show limited robustness against different environment dynamics, as it fails to generalize to tasks where there is considerable variability in the environment from the demonstrations [38].

With the ability to encompass multiple reference motions, AMP decouples task specification from style specification by combining GAIL with extra task objectives [17]. The use of AMP reduces huge efforts in the selection of distance error metrics, phase indicators, and appropriate motion clips. This allows the learning agent to execute tasks that may not be portrayed in the original demonstrations. To enable active style control, Multi-AMP allows for the switching of multiple different style rewards by training multiple discriminators encoding different reference motions in parallel [39].

### 3 Approach

In this section, we describe our method that involves generative adversarial learning of an imitation reward from rough and partial demonstrations.

#### 3.1 Learning Task Reward from Limited Demonstration Information

We consider partial demonstrations that are given in terms of limited state observations, for instance only local velocities of the robot’s base. Formally, the demonstrations are formulated as sequences of  $o_t \in \mathcal{O}$ , where the full state space  $\mathcal{S}$  of the underlying Markov Decision Process can be mapped to the observation space  $\mathcal{O}$  with a function  $\Phi : \mathcal{S} \rightarrow \mathcal{O}$ . We utilize generative adversarial learning for inferring the task reward function from such demonstrated transitions  $(o, o')$  in a reference motion. As such, the task of the discriminator is to distinguish samples of the policy transition distribution  $d^\pi$  from the reference motion distribution  $d^\mathcal{M}$ . The policy  $\pi$  takes on the role of the generator.

The original GAN min-max loss (CEGAN) formulation has shown to suffer from vanishing gradients due to saturation regions of the cross-entropy loss function which slows down training [40]. If the discriminator performs too well and thus becomes saturated, the policy will not be able to learn any information, since it receives a constant penalty for being far away from the demonstrations. For this reason, Peng et al. [17] propose to use the least-squares GAN (LSGAN) loss [41] as a substitute for reward function learning. The LSGAN loss is formulated as

$$\arg \min_D \mathbb{E}_{d^\mathcal{M}} \left[ (D(o, o') - 1)^2 \right] + \mathbb{E}_{d^\pi} \left[ (D(\Phi(s), \Phi(s')) + 1)^2 \right]. \quad (1)$$

The discriminator is defined as a mapping  $D : \mathcal{O} \times \mathcal{O} \mapsto \mathbb{R}$  and can be used, together with  $\Phi$ , as a drop-in replacement for the unknown reward function  $r(s, s')$ . Intuitively, the LSGAN loss forces the discriminator to output +1 for samples from the reference motion and −1 for those from the policy. It not only prevents vanishing gradients but also provides a well-scaled output that eases downstream policy learning. However, when faced with demonstrations that initially seem far away from what the agent can achieve, the discriminator is prone to be driven to optimality, prohibiting a more fine-grained evaluation of the policy transitions with respect to their closeness to the reference motion. Moreover, the LSGAN discriminator output does not directly lead to a practical reward function by itself, since an increase in its value does not always represent close replications of demonstrated transitions. This is a consequence of the least-squares loss symmetry around −1 and +1, therefore a suitable mapping is typically needed to transform the output into a well-behaved reward function. For this reason, we propose to use the Wasserstein loss

$$\arg \min_D -\mathbb{E}_{d^\mathcal{M}} [D(o, o')] + \mathbb{E}_{d^\pi} [D(\Phi(s), \Phi(s'))], \quad (2)$$

especially for highly dynamic motions where the discriminator is more likely to optimally distinguish between the reference and the generated motions. Under conditions of Lipschitz continuity, the Wasserstein loss is an efficient approximation to the earth mover’s distance which effectively measures distance between two probability distributions [42]. In the original Wasserstein GAN (WGAN), Arjovsky et al. [43] enforce Lipschitz continuity by projected gradient descent, i.e. clipping the network weights. Similarly, we apply  $L_2$  regularization on the discriminator for the sake of simplicity. In addition, discriminator weight regularization also controls the scale of its output, which results in stable imitation rewards.

### 3.2 Preventing Mode Collapse in Adversarial Reward Learning

Mode collapse is a common problem in GAN training, which manifests itself by the generator being able to produce only a small set of outputs. In our framework, mode collapse is reflected by the policy trying to replicate only a subset of the reference motion which gives a high reward. The Wasserstein loss can alleviate mode collapse by allowing training of the discriminator to optimality while avoiding vanishing gradients [43]. In fact, if the discriminator does not get stuck in the local minimum, it learns to reject partial behaviors on which the policy stabilizes. As a result, the policy will have to attempt something different, if possible. In addition to the implementation of the Wasserstein loss, we extend the capability of the discriminator by allowing more than one state transition as input, i.e. we extend the input to  $H$  consecutive observations. Note that this is typically not applicable to CEGAN or LSGAN, as a longer horizon makes the discriminator even stronger. By taking more sequential states into account, the policy reduces its chance to resort to the same safe transition patterns that are present in the reference motion.

We denote trajectory segments of length  $H$  preceding time  $t$  by  $o_t^H = (o_{t-H+1}, \dots, o_t)$  for the reference observations and  $s_t^H = (s_{t-H+1}, \dots, s_t)$  for the states induced by the policy. For clarity, we omit the time index in the following. To simplify notation, we write  $\Phi(s^H)$  to express that each state in  $s^H$  is mapped to  $\mathcal{O}$ . In our experiments, we select linear and angular velocities  $v, \omega$  of the robot base in the robot frame, measurement of the gravity vector in the robot frame  $g$ , and the base height  $z$  as the observation space  $\mathcal{O}$ . More information on the state space and demonstration space is detailed in Suppl. B.1. Note that in this example, no joint information is required by the discriminator. This facilitates the process to obtain the expert motion, as one can simply move the robot base by hand along the desired trajectory without any joint actuation.

Using  $H$ -step inputs and a gradient penalty, Eq. 2 turns into

$$\arg \min_D w^D (-\mathbb{E}_{d^M} [D(o^H)] + \mathbb{E}_{d^\pi} [D(\Phi(s^H))]) + w^{\text{GP}} \mathbb{E}_{d^M} [\|\nabla_\Omega D(\Omega) |_{\Omega=o^H}\|_2^2], \quad (3)$$

where the last term denotes the penalty for nonzero gradients on samples from the dataset [17].  $w^D$  and  $w^{\text{GP}}$  denote the weights on the Wasserstein loss and the gradient penalty, respectively. In our experiments, they are set to  $w^D = 0.5$  and  $w^{\text{GP}} = 5.0$  for all tasks.

### 3.3 Reward Formulation

Despite discriminator regularization, due to the unbounded discriminator output, the scale of the reward can be arbitrary which makes it difficult to introduce additional regularization terms for stabilizing the robot motion. Therefore, we normalize the reward to have zero mean and unit variance in the policy training loop by maintaining its running mean  $\hat{\mu}$  and variance  $\hat{\sigma}^2$ . With this formulation, the imitation reward is then given by

$$r^{\text{I}} = \frac{D(\Phi(s^H)) - \hat{\mu}}{\hat{\sigma}}, \quad (4)$$

where  $D(\Phi(s^H))$  denotes the output of the discriminator. In this manner, we are able to limit its range without bounding the discriminator output, which would reduce the benefits gained by introducing the Wasserstein loss.

To increase policy learning efficiency, a common practice is to define a termination condition for rollouts. In our work, an instantaneous environment reset is triggered when a robot base collision against the ground is detected. Since the imitation reward has zero mean and difficult behaviors are likely to result in negative rewards initially, the policy may attempt to end the episode early. To



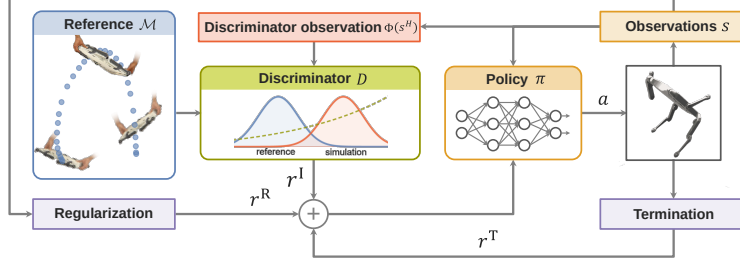


Figure 2: System overview. Given a reference dataset defining the desired base motion, the system trains a discriminator that learns an imitation reward for the policy training. This imitation reward is then combined with a regularization reward and termination penalty to train a policy that enables the robot to replicate the demonstrated motion while maintaining feasible and stable joint actuation.

circumvent this, a termination penalty is imposed at the last transition before a collision happens. As the normalized reward follows a distribution with zero mean and unit variance,  $-5\sigma$  is a lower bound on the reward with a probability greater than 99.99%. We use this to derive a reasonable termination penalty, based on the geometric series, by a high-probability lower bound on the return

$$r^T = \mathbb{I}[s \in \mathcal{T}] \frac{-5\sigma}{1 - \gamma}, \quad (5)$$

where  $\gamma$  is the discount factor,  $\mathcal{T}$  is the set of early termination states, and  $\mathbb{I}[\cdot]$  is the Iverson bracket (1 if true, 0 otherwise). Putting everything together, the total reward that the policy receives encompasses three parts, the imitation reward  $r^I$  defined by the normalized discriminator output, the termination reward  $r^T$ , and the regularization reward  $r^R$  to guarantee stable policy outputs (detailed in Suppl. C)

$$r = w^I(r^I + r^T) + r^R, \quad (6)$$

where  $w^I$  is a motion-specific scaling factor controlling the relative importance of the imitation reward (and the termination penalty) with respect to the regularization terms.

Note that our reward formulation enables the robot to learn highly dynamic skills without any explicitly defined desired-motion-incentivizing reward, as is used in AMP, where an a priori designed reward still has to motivate the policy to execute a specific movement [17]. Figure 2 provides a schematic overview of our method, and an algorithm overview is detailed in Algorithm 1.

---

#### Algorithm 1 WASABI

---

- 1: **Input:** dataset of reference motions  $\mathcal{M}$ , feature map  $\Phi$
  - 2: initialize discriminator  $D$ , policy  $\pi$ , value function  $V$ , state transition buffer  $s^H$ , replay buffer  $B$
  - 3: **for** learning iterations = 1, 2, ... **do**
  - 4:   collect  $N + H$  transitions  $(s_t, a_t, r_t^R, s_{t+1})_{t-H}^{t+N}$  with policy  $\pi$
  - 5:   compute  $r_t^I$  using discriminator outputs  $D(\Phi(s_t^H))$  for  $i = t, \dots, t + N$
  - 6:   calculate transition rewards  $r_t = w^I(r_t^I + r_t^T) + r_t^R$  according to Equations 4, 5, and 6
  - 7:   fill replay buffer  $B$  with  $(s_t, a_t, r_t, s_{t+1}, \Phi(s_t^H))_{t-H}^{t+N}$
  - 8:   **for** policy learning epoch = 1, 2, ...,  $n_\pi$  **do**
  - 9:     sample transition mini-batches  $b^\pi \sim B$
  - 10:    update  $V$  and  $\pi$  by PPO objective or another RL algorithm
  - 11:   **end for**
  - 12:   **for** discriminator learning epoch = 1, 2, ...,  $n_D$  **do**
  - 13:     sample transition mini-batches  $b^\pi \sim B$  and  $b^\mathcal{M} \sim \mathcal{M}$
  - 14:     update discriminator  $D$  using  $b^\pi$  and  $b^\mathcal{M}$  according to the loss associated with Eq. 3
  - 15:   **end for**
  - 16: **end for**
- 

## 4 Experiments

We evaluate WASABI on the Solo 8 robot, an open-source research quadruped robot that performs a wide range of physical actions [44], in simulation and on the real system (Fig. 3). For evaluation,

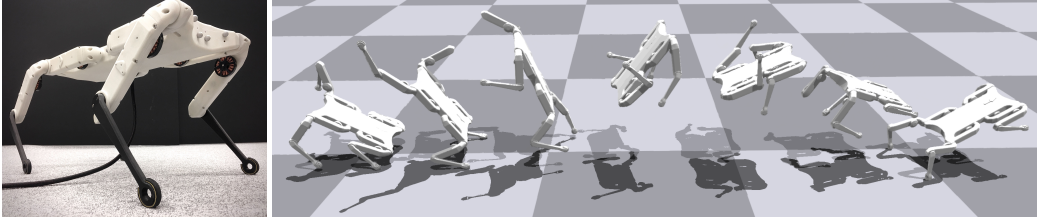


Figure 3: Solo 8 (left). Backflip motion in Isaac Gym (right).

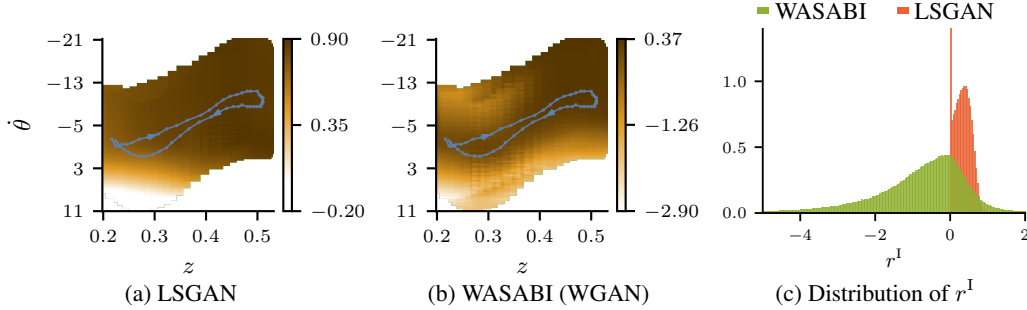


Figure 4: Adversarial imitation rewards for SOLOBACKFLIP. Imitation reward heatmap for LSGAN (a) and WASABI (b) around reference trajectories (blue) generated in varying pitch rate  $\dot{\theta}$  and base height  $z$ . (c) Distribution of imitation rewards for LSGAN and WASABI during training. WASABI provides a more fine-grained reward function.

we introduce 4 different robotics tasks. In SOLOLEAP, the robot is asked to move forward with a jumping motion. SOLOWAVE requires the robot to produce a wave-like locomotion behavior. For SOLOSTANDUP we require the robot to stand up on its hind legs. In SOLOBACKFLIP the robot is asked to generate motions of a full backflip. We provide rough demonstrations of these motions by manually carrying the robot through the motion and recording only the base information. The demonstrations are then used to infer an adversarial imitation reward for training a control policy, as outlined in Sec. 3.1. An overview of the desired movements is provided in Suppl. F, we also provide further ablation studies in Suppl. H.

In all of our experiments, we use Proximal Policy Optimization (PPO) [45] in Isaac Gym [46] and make use of domain randomization [47] for sim-to-real transfer. Further details on the training procedure can be found in Suppl. A.

#### 4.1 Induced Imitation Reward Distributions

The LSGAN loss is proposed to alleviate the saturation problem that is encountered for the CEGAN loss. Yet, as outlined in Sec. 3.1, it does not directly yield a practical reward function. Peng et al. [17] remedy this by using  $r^I = \max[0, 1 - 0.25(D(\Phi(s), \Phi(s')) - 1)^2]$  to map the discriminator output to the imitation reward and bound it between 0 and 1. However, with the effective clipping at 0, information about the distance from the policy to the demonstration transitions is lost with discriminator prediction smaller than  $-1$  (Fig. 4c). In addition, we show in Fig. 4b that the imitation reward learned using LSGAN yields a less informative signal for policy training, which is rather uniformly distributed across pitch rate  $\dot{\theta}$  and base height  $z$  dimensions. In comparison, WASABI can use the discriminator output directly, learning a more characteristic reward function across the state space where reference trajectories are clearly outlined to yield high rewards in contrast to the off-trajectory states.

#### 4.2 Learning to Mimic Rough Demonstrations

Since we record the base motion of the robot carried by a human demonstrator, we do not have access to a reward function evaluating learned behaviors or measuring the closeness between the demonstrated and the policy trajectories. In addition, these trajectories are largely misaligned. For

Method	SOLOLEAP	SOLOWAVE	SOLOSTANDUP	SOLOBACKFLIP
WASABI	<b>131.70 <math>\pm</math> 16.44</b>	<b>247.29 <math>\pm</math> 11.59</b>	<b>351.13 <math>\pm</math> 88.60</b>	<b>477.43 <math>\pm</math> 56.77</b>
LSGAN	<b>155.31 <math>\pm</math> 18.10</b>	<b>230.91 <math>\pm</math> 5.95</b>	678.21 $\pm$ 6.71	813.76 $\pm$ 19.75
Stand Still	216.41	460.15	494.40	877.74

Table 1: Comparison of performances for LSGAN and WASABI trained with hand-held demonstrations in terms of **DTW distance**  $d^{\text{DTW}}$  (lower is better), successful runs are in **bold** font. As a reference, we provide also  $d^{\text{DTW}}$  of a constantly standing trajectory.

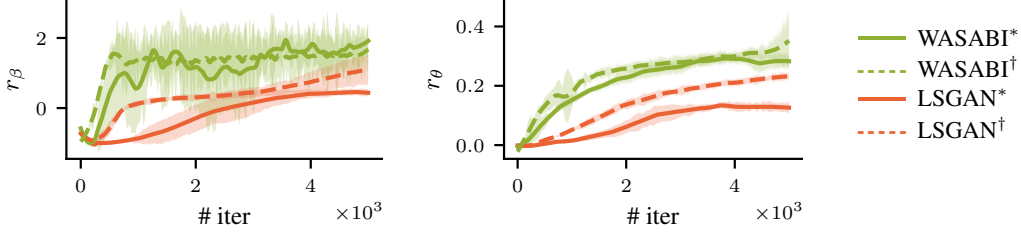


Figure 5: Performance of WASABI and LSGAN in terms of the handcrafted task reward for SOLOSTANDUP (left) and SOLOBACKFLIP (right). Dashed lines indicate partial information ( $\dagger$ ).

this reason, we make use of Dynamic Time Warping (DTW) [48] with the  $L_2$  norm metric for comparing policy trajectories and reference demonstrations. DTW allows us to match and compute the distance between the trajectories in a time-consistent manner (Fig. 1). Concretely, we use  $\mathbb{E}[d^{\text{DTW}}(\Phi(\tau_\pi), \tau_{\mathcal{M}})]$  as the evaluation metric, where  $\tau_\pi \sim d^\pi$  is a state trajectory from a policy rollout and  $\tau_{\mathcal{M}} \sim d^{\mathcal{M}}$  denotes a reference motion from the dataset. We provide further details about this metric in Suppl. G. In Table 1 we compare performances in simulation for the different reference motions.

In order to confirm that WASABI is indeed able to extract a sensible reward function that motivates the desired motion, we compare the performance of LSGAN and WASABI in SOLOSTANDUP and SOLOBACKFLIP using an expert baseline that is trained on a handcrafted task reward for generating demonstrations in simulation. Details on the handcrafted task reward formulation are given in Suppl. D. The learned policies are evaluated with the same task rewards that are used to obtain the expert policies. A comparison of training performance curves in terms of the corresponding handcrafted task rewards is detailed in Fig. 5. In Table 2 we show the performance evaluation of the best runs. Observe that the policies trained by WASABI perform comparably to the expert policies trained with the handcrafted rewards. Interestingly, learning from partial state information may sometimes facilitate policy learning, since a decrease in discriminator observation dimensions could potentially alleviate the problem of discriminator becoming too strong as indicated in Fig. 5.

### 4.3 Evaluation on Real Robot

To evaluate our method on real system, we trained policies for sim-to-real transfer with WASABI for the SOLOLEAP, SOLOWAVE and SOLOBACKFLIP. The Solo 8 robot is powered by an external battery and driven by a controller on an external operating machine. It receives root state estimation

Method	SOLOSTANDUP $\dagger$	SOLOSTANDUP*	SOLOBACKFLIP $\dagger$	SOLOBACKFLIP*
WASABI	<b>1.54 <math>\pm</math> 0.51</b>	<b>1.68 <math>\pm</math> 0.51</b>	<b>0.36 <math>\pm</math> 0.05</b>	<b>0.28 <math>\pm</math> 0.02</b>
LSGAN	1.07 $\pm$ 0.5	0.44 $\pm$ 0.14	0.12 $\pm$ 0.01	0.06 $\pm$ 0.01
Handcrafted	<b>2.24 <math>\pm</math> 0.05</b>		<b>0.77 <math>\pm</math> 0.04</b>	

Table 2: Performance comparison in terms of handcrafted **task reward** (higher is better). We denote with \* where the full robot configuration is given to the discriminator and  $\dagger$  where only base information is given. Successful runs are in **bold** font. Std-dev. is over 5 independent random seeds.

using 10 markers attached around the base which are tracked using a Vicon motion capture system operating at 100 Hz. During deployment, we recorded the robot base information for evaluation by  $d^{\text{DTW}}$ . As detailed in Suppl. E, the policy observation space, reward and training hyperparameters are adapted to facilitate sim-to-real transfer for these tasks specifically. The resulting performance on the real system, as shown in Table 3, resembles the performance obtained in simulation.

	SOLOLEAP	SOLOWAVE	SOLOBACKFLIP
WASABI (Real)	$153.64 \pm 7.08$	$215.38 \pm 21.82$	$504.26 \pm 18.90$
WASABI (Sim)	$131.70 \pm 16.44$	$247.29 \pm 11.59$	$477.43 \pm 56.77$

Table 3: Sim-to-real performance on the Solo 8 in terms of DTW distance (lower is better). Values are computed from the recorded data of the learned policies with respect to the reference trajectories.

## 5 Conclusion

In this work, we propose a generative adversarial method for inferring reward functions that is capable of learning agile skills from partial and physically incompatible demonstrations without any a priori known reward terms. Our results indicate that this method is capable of extracting robust policies that are able to transfer to the real system with the help of additional regularization terms. Furthermore, our experiments confirm that adversarial imitation learning using the LSGAN is able to replicate motions that are more closely achievable. Thus, it fits style transfer settings where a task reward still needs to motivate the desired motion. For highly agile or incompatible motions which initially seem far away from the robot’s capability, WASABI outperforms LSGAN by successful and faithful replication of roughly demonstrated behaviors.

## 6 Limitations

While saving the effort of developing a specific task reward that motivates desired motions, providing a good evaluation metric in terms of a distance to the reference motion is not straightforward for generic rough demonstrations. Although DTW is a feasible option, it still requires a reasonable distance metric and careful choice of the warping procedure, which might be task-dependent. Moreover, since our method works with rough demonstrations, even a good distance metric to the reference may not be helpful in informing about closeness to feasible, desirable motions from the robot’s perspective. Finally, we did not intensively study to what extent our method is robust against the degree of incompatibility of the demonstrations.

## Acknowledgments

Georg Martius is a member of the Machine Learning Cluster of Excellence, EXC number 2064/1 – Project number 390727645. We acknowledge the support from the German Federal Ministry of Education and Research (BMBF) through the Tübingen AI Center (FKZ: 01IS18039B). The authors thank the International Max Planck Research School for Intelligent Systems (IMPRS-IS) for supporting Marin Vlastelica and Sebastian Blaes, and Max Planck ETH Center for Learning Systems for supporting Jonas Frey.

## References

- [1] M. Raibert, K. Blankespoor, G. Nelson, and R. Playter. Bigdog, the rough-terrain quadruped robot. *IFAC Proceedings Volumes*, 41(2):10822–10825, 2008.
- [2] J. Di Carlo, P. M. Wensing, B. Katz, G. Bledt, and S. Kim. Dynamic locomotion in the mit cheetah 3 through convex model-predictive control. In *2018 IEEE/RSJ International Conference on Intelligent Robots and Systems (IROS)*, pages 1–9. IEEE, 2018.
- [3] J. Hwangbo, J. Lee, A. Dosovitskiy, D. Bellicoso, V. Tsounis, V. Koltun, and M. Hutter. Learning agile and dynamic motor skills for legged robots. *Science Robotics*, 4(26):eaau5872, 2019.
- [4] J. Lee, J. Hwangbo, L. Wellhausen, V. Koltun, and M. Hutter. Learning quadrupedal locomotion over challenging terrain. *Science robotics*, 5(47):eabc5986, 2020.
- [5] A. Kumar, Z. Fu, D. Pathak, and J. Malik. RMA: Rapid motor adaptation for legged robots. In *Robotics: Science and Systems XVII (RSS)*, 2021.
- [6] T. Miki, J. Lee, J. Hwangbo, L. Wellhausen, V. Koltun, and M. Hutter. Learning robust perceptive locomotion for quadrupedal robots in the wild. *Science Robotics*, 7(62):eabk2822, 2022.
- [7] D. A. Pomerleau. Efficient training of artificial neural networks for autonomous navigation. *Neural Computation*, 3(1):88–97, 1991.
- [8] F. Torabi, G. Warnell, and P. Stone. Behavioral cloning from observation. *ArXiv*, abs/1805.01954, 2018.
- [9] S. Ross, G. Gordon, and D. Bagnell. A reduction of imitation learning and structured prediction to no-regret online learning. In *Proceedings of the Fourteenth International Conference on Artificial Intelligence and Statistics*, pages 627–635. JMLR Workshop and Conference Proceedings, 2011.
- [10] A. Hussein, M. M. Gaber, E. Elyan, and C. Jayne. Imitation learning: A survey of learning methods. *ACM Computing Surveys (CSUR)*, 50(2):1–35, 2017.
- [11] B. D. Ziebart, A. L. Maas, J. A. Bagnell, A. K. Dey, et al. Maximum entropy inverse reinforcement learning. In *AAAI*, volume 8, pages 1433–1438. Chicago, IL, USA, 2008.
- [12] E. Bashir and M. Luštrek. Inverse reinforcement learning through max-margin algorithm. In *Intelligent Environments 2021: Workshop Proceedings of the 17th International Conference on Intelligent Environments*, volume 29, page 190. IOS Press, 2021.
- [13] D. Garg, S. Chakraborty, C. Cundy, J. Song, and S. Ermon. Iq-learn: Inverse soft-q learning for imitation. *Advances in Neural Information Processing Systems*, 34, 2021.
- [14] P. Abbeel and A. Y. Ng. Apprenticeship learning via inverse reinforcement learning. In *Proceedings of the Twenty-first International Conference on Machine Learning*, page 1, 2004.
- [15] J. Ho and S. Ermon. Generative adversarial imitation learning. In *Advances in Neural Information Processing Systems*, volume 29, 2016.
- [16] I. Goodfellow, J. Pouget-Abadie, M. Mirza, B. Xu, D. Warde-Farley, S. Ozair, A. Courville, and Y. Bengio. Generative adversarial networks. In *Advances in Neural Information Processing Systems*, volume 3, 06 2014.



- [17] X. B. Peng, Z. Ma, P. Abbeel, S. Levine, and A. Kanazawa. AMP: Adversarial motion priors for stylized physics-based character control. *ACM Transactions on Graphics (TOG)*, 40(4):1–20, 2021.
- [18] D. Pathak, D. Gandhi, and A. Gupta. Self-supervised exploration via disagreement. In *International Conference on Machine Learning*, pages 5062–5071. PMLR, 2019.
- [19] Q. Cai, Z. Yang, C. Jin, and Z. Wang. Provably efficient exploration in policy optimization. In *International Conference on Machine Learning*, pages 1283–1294. PMLR, 2020.
- [20] A. Billard, S. Calinon, R. Dillmann, and S. Schaal. Survey: Robot programming by demonstration. Technical report, Springer, 2008.
- [21] B. D. Argall, S. Chernova, M. Veloso, and B. Browning. A survey of robot learning from demonstration. *Robotics and Autonomous Systems*, 57(5):469–483, 2009.
- [22] S. Schaal. Learning from demonstration. *Advances in Neural Information Processing Systems*, 9, 1996.
- [23] C. G. Atkeson and S. Schaal. Robot learning from demonstration. In *ICML*, volume 97, pages 12–20, 1997.
- [24] S. Schaal. Is imitation learning the route to humanoid robots? *Trends in Cognitive Sciences*, 3(6):233–242, 1999.
- [25] S. Calinon, F. D’halluin, E. L. Sauser, D. G. Caldwell, and A. G. Billard. Learning and reproduction of gestures by imitation. *IEEE Robotics & Automation Magazine*, 17(2):44–54, 2010.
- [26] S. M. Khansari-Zadeh and A. Billard. Learning stable nonlinear dynamical systems with gaussian mixture models. *IEEE Transactions on Robotics*, 27(5):943–957, 2011.
- [27] A. J. Ijspeert, J. Nakanishi, H. Hoffmann, P. Pastor, and S. Schaal. Dynamical movement primitives: learning attractor models for motor behaviors. *Neural Computation*, 25(2):328–373, 2013.
- [28] F. Codevilla, E. Santana, A. M. López, and A. Gaidon. Exploring the limitations of behavior cloning for autonomous driving. In *Proceedings of the IEEE/CVF International Conference on Computer Vision*, pages 9329–9338, 2019.
- [29] Y. Lee, S. Kim, and J. Lee. Data-driven biped control. *ACM Trans. Graph.*, 29(4), jul 2010. ISSN 0730-0301.
- [30] L. Liu, K. Yin, M. van de Panne, T. Shao, and W. Xu. Sampling-based contact-rich motion control. *ACM SIGGRAPH 2010 papers*, 2010.
- [31] L. Liu, M. V. D. Panne, and K. Yin. Guided learning of control graphs for physics-based characters. *ACM Transactions on Graphics (TOG)*, 35(3):1–14, 2016.
- [32] X. B. Peng, P. Abbeel, S. Levine, and M. van de Panne. Deepmimic: Example-guided deep reinforcement learning of physics-based character skills. *ACM Transactions on Graphics (TOG)*, 37(4):1–14, 2018.
- [33] S. Lee, M. Park, K. Lee, and J. Lee. Scalable muscle-actuated human simulation and control. *ACM Transactions On Graphics (TOG)*, 38(4):1–13, 2019.
- [34] X. B. Peng, A. Kanazawa, J. Malik, P. Abbeel, and S. Levine. Sfv: Reinforcement learning of physical skills from videos. *ACM Transactions On Graphics (TOG)*, 37(6):1–14, 2018.
- [35] J. Merel, Y. Tassa, D. TB, S. Srinivasan, J. Lemmon, Z. Wang, G. Wayne, and N. Heess. Learning human behaviors from motion capture by adversarial imitation. *arXiv preprint arXiv:1707.02201*, 2017.
- [36] Z. Wang, J. S. Merel, S. E. Reed, N. de Freitas, G. Wayne, and N. Heess. Robust imitation of diverse behaviors. *Advances in Neural Information Processing Systems*, 30, 2017.

- [37] R. Jena and K. P. Sycara. Loss-annealed gail for sample efficient and stable imitation learning. *ArXiv*, abs/2001.07798, 2020.
- [38] J. Fu, K. Luo, and S. Levine. Learning robust rewards with adversarial inverse reinforcement learning. *arXiv preprint arXiv:1710.11248*, 2017.
- [39] E. Vollenweider, M. Bjelonic, V. Klemm, N. Rudin, J. Lee, and M. Hutter. Advanced skills through multiple adversarial motion priors in reinforcement learning. *arXiv preprint arXiv:2203.14912*, 2022.
- [40] M. Arjovsky and L. Bottou. Towards principled methods for training generative adversarial networks. *arXiv preprint arXiv:1701.04862*, 2017.
- [41] X. Mao, Q. Li, H. Xie, R. Y. Lau, Z. Wang, and S. Paul Smolley. Least squares generative adversarial networks. In *Proceedings of the IEEE International Conference on Computer Vision*, pages 2794–2802, 2017.
- [42] Y. Rubner, C. Tomasi, and L. J. Guibas. A metric for distributions with applications to image databases. In *Sixth international conference on computer vision (IEEE Cat. No. 98CH36271)*, pages 59–66. IEEE, 1998.
- [43] M. Arjovsky, S. Chintala, and L. Bottou. Wasserstein gan. *ArXiv*, abs/1701.07875, 2017.
- [44] F. Grimminger, A. Meduri, M. Khadiv, J. Viereck, M. Wüthrich, M. Naveau, V. Berenz, S. Heim, F. Widmaier, T. Flayols, J. Fiene, A. Badri-Spröwitz, and L. Righetti. An open torque-controlled modular robot architecture for legged locomotion research. *IEEE Robotics and Automation Letters*, 5(2):3650–3657, 2020. doi:10.1109/LRA.2020.2976639.
- [45] J. Schulman, F. Wolski, P. Dhariwal, A. Radford, and O. Klimov. Proximal policy optimization algorithms. *arXiv preprint arXiv:1707.06347*, 2017.
- [46] V. Makoviychuk, L. Wawrzyniak, Y. Guo, M. Lu, K. Storey, M. Macklin, D. Hoeller, N. Rudin, A. Allshire, A. Handa, et al. Isaac gym: High performance gpu-based physics simulation for robot learning. *arXiv preprint arXiv:2108.10470*, 2021.
- [47] J. Tobin, R. Fong, A. Ray, J. Schneider, W. Zaremba, and P. Abbeel. Domain randomization for transferring deep neural networks from simulation to the real world. In *2017 IEEE/RSJ International Conference on Intelligent Robots and Systems (IROS)*, pages 23–30. IEEE, 2017.
- [48] D. J. Berndt and J. Clifford. Using dynamic time warping to find patterns in time series. In *KDD Workshop*, 1994.

# Supplementary for Learning Agile Skills via Adversarial Imitation of Rough Partial Demonstrations

## A Training Details

### A.1 Training Parameters

The learning networks and algorithm are implemented in PyTorch 1.10 with CUDA 11.3. Adam is used as the optimizer for the policy and value function with an adaptive learning rate with a KL divergence target of 0.01. The optimizer for the discriminator is SGD. The discount factor  $\gamma$  is set to 0.99, the clip range  $\epsilon$  is set to 0.2, and the entropy coefficient  $\alpha$  is set to 0.01. The policy runs at 50 Hz. All training is done by collecting experiences from 4096 uncorrelated instances of the simulator in parallel. Most of the experiments are executed on the cluster of Max Planck Institute for Intelligent Systems with NVIDIA A100 and Tesla V100 GPUs. In this setting, one run with 5000 iterations with the specified compute settings and devices completes within 2 hours. The information is summarized in Table S4.

Table S4: Training parameters

Parameter	Symbol	Value
step time seconds	—	0.02
max episode time seconds	—	20
max iterations	—	5000
steps per iteration	—	24
policy learning epochs	—	5
policy mini-batches	—	4
KL divergence target	—	0.01
discount factor	$\gamma$	0.99
clip range	$\epsilon$	0.2
entropy coefficient	$\alpha$	0.01
discriminator weight decay	$wd^D$	0.001
discriminator momentum	—	0.05
discriminator gradient penalty coefficient	—	5.0
discriminator learning epochs	—	1
discriminator mini-batches	—	80
Wasserstein loss weight	$w^D$	0.5
gradient penalty weight	$w^{GP}$	5.0
parallel training environments	—	4096
number of seeds	—	5
approximate training hours	—	2
policy learning rate	$lr^\pi$	grid-searched
discriminator learning rate	$lr^D$	grid-searched
discriminator observation horizon	$H$	grid-searched
imitation reward relative importance	$w^I$	grid-searched

Note that policy learning rate, discriminator learning rate, discriminator observation horizon, and imitation reward relative importance are grid-searched and optimized in different tasks. We report the value used for evaluation in Sec. 4 in Table S5.

### A.2 Network Architecture

The network architecture is detailed in Table S6, where  $H$  denotes the discriminator observation horizon.

Table S5: Task-specific parameters

Section	Task	Method	$lr^\pi$	$lr^D$	$H$	$w^I$
Sec. 4.1 (Sim)	SOLOBACKFLIP	LSGAN	$1.0 \times 10^{-6}$	$1.0 \times 10^{-4}$	2	0.8
		WASABI	$1.0 \times 10^{-7}$	$1.0 \times 10^{-7}$	16	4.0
Sec. 4.2 (Sim)	SOLOLEAP	LSGAN	$1.0 \times 10^{-4}$	$1.0 \times 10^{-4}$	2	0.8
		WASABI	$1.0 \times 10^{-7}$	$5.0 \times 10^{-8}$	2	8.0
	SOLOWAVE	LSGAN	$1.0 \times 10^{-6}$	$1.0 \times 10^{-4}$	4	0.8
		WASABI	$1.0 \times 10^{-6}$	$5.0 \times 10^{-8}$	4	0.8
	SOLOSTANDUP	LSGAN	$1.0 \times 10^{-4}$	$1.0 \times 10^{-4}$	2	0.8
		WASABI	$1.0 \times 10^{-7}$	$1.0 \times 10^{-7}$	4	4.0
	SOLOBACKFLIP	LSGAN	$1.0 \times 10^{-6}$	$1.0 \times 10^{-4}$	2	0.8
		WASABI	$1.0 \times 10^{-7}$	$1.0 \times 10^{-7}$	16	4.0
	SOLOSTANDUP <sup>†</sup>	LSGAN	$5.0 \times 10^{-5}$	$5.0 \times 10^{-5}$	8	0.8
		WASABI	$1.0 \times 10^{-7}$	$5.0 \times 10^{-7}$	2	4.0
	SOLOSTANDUP*	LSGAN	$1.0 \times 10^{-4}$	$1.0 \times 10^{-5}$	8	0.8
		WASABI	$5.0 \times 10^{-7}$	$1.0 \times 10^{-7}$	2	4.0
	SOLOBACKFLIP <sup>†</sup>	LSGAN	$5.0 \times 10^{-5}$	$1.0 \times 10^{-5}$	8	0.8
		WASABI	$1.0 \times 10^{-7}$	$5.0 \times 10^{-8}$	2	4.0
	SOLOBACKFLIP*	LSGAN	$1.0 \times 10^{-4}$	$1.0 \times 10^{-5}$	8	0.8
		WASABI	$1.0 \times 10^{-7}$	$5.0 \times 10^{-8}$	2	0.8
Sec. 4.3 (Real)	SOLOLEAP	WASABI	$1.0 \times 10^{-3}$	$5.0 \times 10^{-7}$	2	0.1
	SOLOWAVE	WASABI	$1.0 \times 10^{-3}$	$5.0 \times 10^{-7}$	2	0.1
	SOLOBACKFLIP	WASABI	$1.0 \times 10^{-3}$	$5.0 \times 10^{-7}$	2	0.4

Table S6: Network architecture

Network	Symbol	Type	Shape	Activation
policy	$\pi$	MLP	68, 128, 128, 128, 8	Exponential Linear Unit (ELU)
value function	$V$	MLP	68, 128, 128, 128, 1	Exponential Linear Unit (ELU)
discriminator	$D$	MLP	10H, 512, 256, 1	Rectified Linear Unit (ReLU)

### A.3 Domain Randomization

Two types of domain randomization techniques are applied during training to improve policy performance when transferring from simulation to the real system.

On the one hand, the base mass of the parallel training instances is perturbed with an additional weight  $m' \sim \mathcal{U}(-0.5, 1.0)$ , where  $\mathcal{U}$  denotes uniform distribution. On the other hand, random pushing is also applied every 15 seconds on the robot base by forcing its horizontal linear velocity to be set randomly within  $v_{xy} \sim \mathcal{U}(-0.5, 0.5)$ .

## B Model Representation

### B.1 Discriminator Observation

Table S7 lists the extracted features sent to the discriminator.

For discriminator observation horizon  $H > 1$ , the entries are concatenated to a vector of size  $10H$ . The resulting features are then normalized and used as inputs to the discriminator network.

### B.2 States, Actions, and Rewards

In our work, we use a universal set of states as the policy observations for all tasks. It has 68 dimensions and consists of the same set of state measurements of two consecutive steps as detailed in

Table S7: Discriminator observation space

Entry	Symbol	Dimensions
base linear velocity	$v$	0:3
base angular velocity	$\omega$	3:6
projected gravity	$g$	6:9
base height	$z$	9:10

Table S8: Policy observation space

Entry	Symbol	Dimensions	noise level $b$
base linear velocity	$v$	0:3	0.2
base angular velocity	$\omega$	3:6	0.05
projected gravity	$g$	6:9	0.05
base height	$z$	9:10	0.01
joint positions	$q$	10:18	0.01
joint velocities	$\dot{q}$	18:26	0.75
last actions	$a'$	26:34	0.0

Table S8. The observation space is composed of base linear and angular velocities  $v, \omega$  in the robot frame, measurement of the gravity vector in the robot frame  $g$ , base height  $z$ , joint positions  $q$  and velocities  $\dot{q}$ , and the most recent actions  $a'$ .

The noise level  $b$  denotes the artificial noise added during training to increase the policy robustness. Note again that the policy receives the observation collection for two consecutive steps. This is not necessarily optimal for all the tasks as less information would suffice for easier tasks. For simplicity, we use this fixed set of observations for all experiments.

The action space is of 8 dimensions and encodes the target joint position for each of the 8 actuators.

## C Regularization Reward Functions

The regularization reward functions contain only regularization terms whose formulation is detailed below. A universal set of involved hyperparameters is used across different motions and is summarized in Table S9.

### C.1 Action Rate

$$r_{ar} = w_{ar} \|a' - a\|_2^2, \quad (S7)$$

where  $w_{ar}$  denotes the weight of the action rate reward,  $a'$  and  $a$  denote the previous and current actions.

### C.2 Joint Acceleration

$$r_{qa} = w_{qa} \left\| \frac{\dot{q}' - \dot{q}}{\Delta t} \right\|_2^2, \quad (S8)$$

where  $w_{qa}$  denotes the weight of the joint acceleration reward,  $\dot{q}'$  and  $\dot{q}$  denote the previous and current joint velocity,  $\Delta t$  denotes the step time interval.

Table S9: Regularization reward hyperparameters

Hyperparameter	$w_{ar}$	$w_{qa}$	$w_{qT}$	$w_{\dot{\phi}}$	$w_{\dot{\psi}}$	$w_{\dot{y}}$
Value	-0.005	$-1.25 \times 10^{-8}$	$-1.25 \times 10^{-6}$	-0.001	-0.001	-0.001



### C.3 Joint Torque

$$r_{qT} = w_{qT} \|T\|_2^2, \quad (\text{S9})$$

where  $w_{qT}$  denotes the weight of the joint torque reward,  $T$  denotes the joint torques.

### C.4 Angular Velocity $x$

$$r_{\dot{\phi}} = w_{\dot{\phi}} \|\dot{\phi}\|_2^2, \quad (\text{S10})$$

where  $w_{\dot{\phi}}$  denotes the weight of the angular velocity  $x$  reward,  $\dot{\phi}$  denotes the base roll rate.

### C.5 Angular Velocity $z$

$$r_{\dot{\psi}} = w_{\dot{\psi}} \|\dot{\psi}\|_2^2, \quad (\text{S11})$$

where  $w_{\dot{\psi}}$  denotes the weight of the angular velocity  $z$  reward,  $\dot{\psi}$  denotes the base yaw rate.

### C.6 Linear Velocity $y$

$$r_{\dot{y}} = w_{\dot{y}} \|\dot{y}\|_2^2, \quad (\text{S12})$$

where  $w_{\dot{y}}$  denotes the weight of the linear velocity  $y$  reward,  $\dot{y}$  denotes the base lateral velocity.

## D Handcrafted Task Reward

### D.1 Upright Stand for SOLOSTANDUP

The robot is encouraged to stand up by rewarding the pitch angle of the base, the base height, and the standing on only the two hind legs.

$$r_{\beta} = w_{\theta_z} \theta_z + w_z z + w_g c_g, \quad (\text{S13})$$

where  $\theta_z$  denotes the pitch angle with respect to the global  $z$ -axis,  $w_{\theta_z} = 1.0$  denotes its weight.  $z$  denotes the base height and  $w_z = 3.0$  denotes its weight.  $c_g$  is a binary variable that takes 1 if the front legs have no contact with the ground,  $w_g = 2.0$  denotes its weight.

### D.2 Traversed Angle for SOLOBACKFLIP

The robot is encouraged to perform back-flipping by rewarding its traversed angle around the  $y$ -axis while in the air. This reward will be given only when the robot lands.

$$r_{\theta} = w_{\theta} \theta \llbracket s \in \mathcal{L} \rrbracket, \quad (\text{S14})$$

where  $w_{\theta} = 5.0$  denotes the weight of the traversed angle reward,  $\theta$  denotes the traversed angle around  $y$ -axis while in the air.  $\mathcal{L}$  is the set of robot landing states, and  $\llbracket \cdot \rrbracket$  is the Iverson bracket.

## E Sim-to-Real Transfer

To deploy the learned policy on the real system, the following adaptations are made to reduce the sim-to-real gap.

Table S10: Regularization reward adaptation

Task	$w_{ar}$	$w_{q_a}$	$w_{q_T}$	$w_{\dot{\phi}}$	$w_{\dot{\psi}}$	$w_{\dot{y}}$	$w_{t_f}$
SOLOLEAP	-0.01	$-2.5 \times 10^{-7}$	$-2.5 \times 10^{-5}$	-0.05	-0.05	-0.05	0.1
SOLOWAVE	-0.01	$-2.5 \times 10^{-7}$	$-2.5 \times 10^{-5}$	-0.01	-0.01	-0.01	0.05
SOLOBACKFLIP	-0.01	$-2.5 \times 10^{-7}$	$-1.0 \times 10^{-5}$	-0.02	-0.02	-0.02	0.0



Figure S6: Hand-held motion demonstration for SOLOBACKFLIP. Note that the robot joints are not actuated and only base information is recorded.

### E.1 Observation Space Adaptation

Generally, policies trained in simulation suffer from poor performance when transferred to the real system. One primary reason of such failures is the incorrectly modeled system dynamics. As a result, the state transitions observed in simulation may divert from reality. On account of this, instead of using two consecutive steps of the observation collection in Suppl. B.2, only the observation at the current time step is used. The resulting policy observation space has thus only 34 entries and is detailed in Table S8.

### E.2 Training Hyperparameter Adaptation

Some training hyperparameters are further refined and specifically adapted for the deployment on the real system as detailed in Table S5.

### E.3 Reward Adaptation

To generate stable joint actuation and achieve task-specific high performance, a feet air time regularization reward is introduced to motivate higher off-ground steps during robot movement.

$$r_{t_f} = w_{t_f} \sum_{i=1}^4 t_{f_i} \llbracket f_i \in \mathcal{C} \rrbracket, \quad (\text{S15})$$

where  $w_{t_f}$  denotes the weight of the feet air time reward,  $t_{f_i}$  denotes the time foot  $i$  stays in the air.  $\mathcal{C}$  is the set of foot states touching the ground, and  $\llbracket \cdot \rrbracket$  is the Iverson bracket. The resulting task-specific regularization reward setting is provided in Table S10.

## F Motions

### F.1 Data Collection

The reference motions containing only the base information (as detailed in Sec. B.1) are performed by a human demonstrator and recorded using a Vicon motion capture system as illustrated in Figure S6. For each motion, 20 trajectories are recorded and used as the reference motion dataset.

### F.2 Motion details

We provide sequences of the respective motions that we learn in this work in Fig. S7.

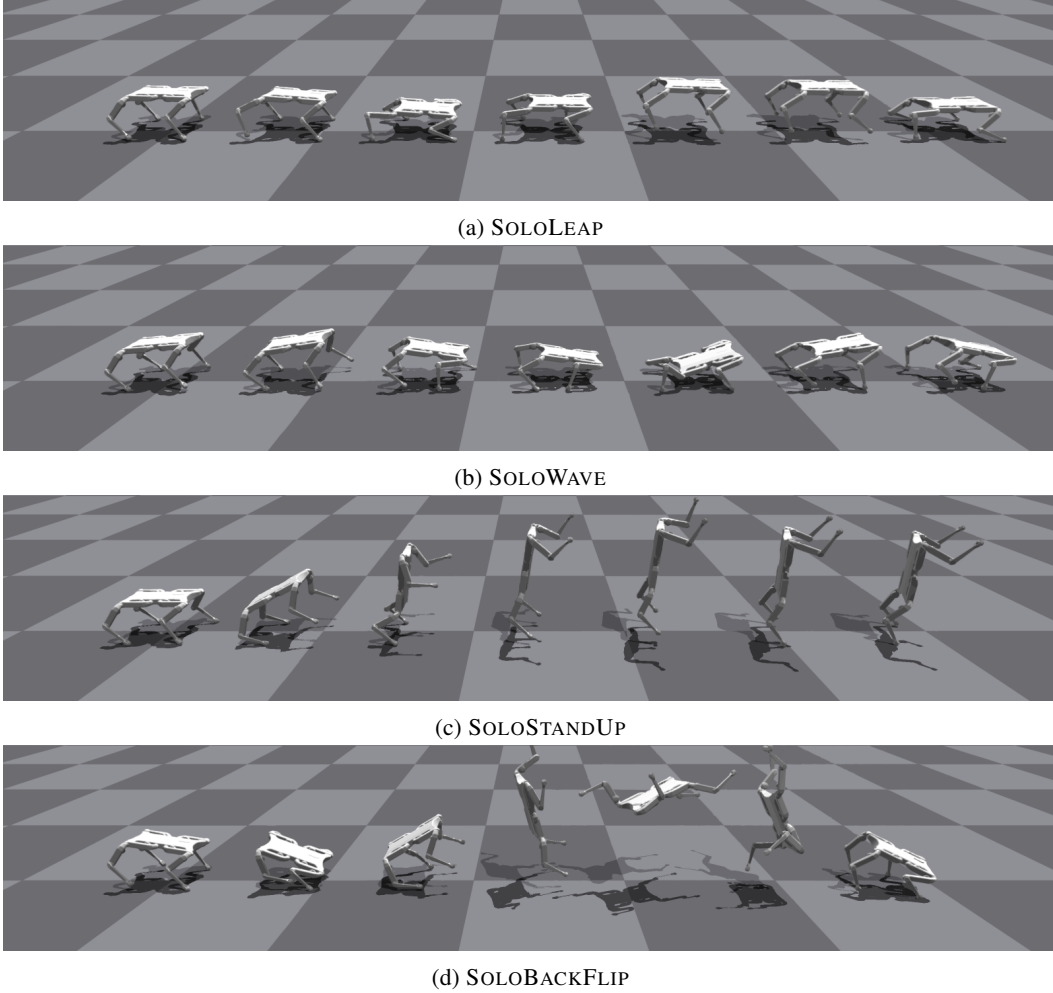


Figure S7: Task motion sequences induced by the learned policies in simulation.

## G Dynamic Time Warping Evaluation

We make use of an imitation reward as outlined in Sec. 3.1 for learning policies from rough reference trajectories. Since the reference trajectories might not be completely achievable, either in terms of time consistency or the actual sequence of states that are infeasible, a simple evaluation metric such as the direct  $L_2$  distance between policy and reference trajectories is not applicable. Furthermore, a learned policy might replicate the demonstrated motion perfectly in a certain sub-sequence, however, in the absence of proper alignment and synchronization, it would incur a large penalty in terms of a simple distance metric.

To account for the potential misalignment in the policy vs. reference trajectories, the policy trajectories need to be synchronized to the reference. Dynamic Time Warping (DTW) is an algorithm that computes an alignment between two sequences such that a distance measure between the elements of the sequences is minimized, under a set of matching constraints. This can be computed efficiently via dynamic programming, an example of such a matching is given for our case in Fig. 1.

For the distance measure between the matched elements of the sequences we use the standard  $L_2$  distance, and for the matching computation we use the ‘dtw’ Python package [1] with the Mori asymmetric step pattern [2] and open-ended matching. The asymmetric step pattern constrains the type of element matches that can happen between the trajectories and also makes it possible for some elements to be skipped, while open-ended matching allows for ends of trajectories to be matched to

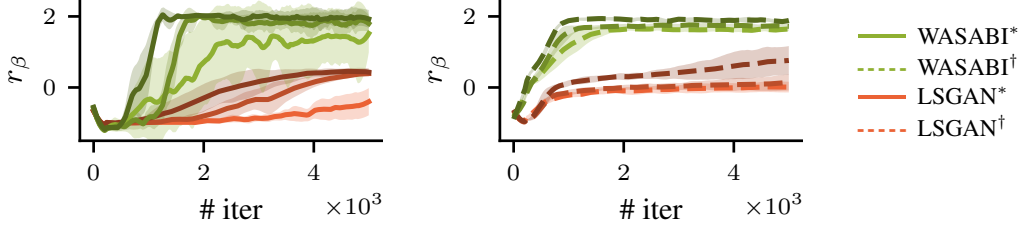


Figure S8: Performance of LSGAN (left) and WASABI (right) in terms of the handcrafted task reward for SOLOSTANDUP with different discriminator observation horizons (light  $H = 2$ , middle  $H = 4$ , dark  $H = 8$ ). Solid lines indicate full information (\*) and dashed lines indicate partial information (†).

an earlier time point which is necessary in order to account for time shift. The resulting measure is denoted with  $d^{\text{DTW}}$ .

As clarified in Sec. 4, we calculate the expectation

$$\mathbb{E} [d^{\text{DTW}}(\Phi(\tau_\pi), \tau_{\mathcal{M}})] \quad (\text{S16})$$

as the evaluation metric, where  $\tau_\pi \sim d^\pi$  is a state trajectory drawn from a policy rollout distribution and  $\tau_{\mathcal{M}} \sim d^{\mathcal{M}}$  denotes a reference motion from the dataset. With the same notation as in Sec. 3.2, the function  $\Phi$  maps each state in the state trajectory of the policy to the reference observation space  $\mathcal{O}$ . In practice, we estimate this by drawing 20 policy rollouts, comparing each of the 20 rollouts with 20 collected reference trajectories and taking the mean. Note that  $d^{\text{DTW}}$  is not comparable across different tasks, thus we provide a pure standing reference in Table 1.

## H Ablation Studies

To prevent mode collapse, we extend the capability of the discriminator by allowing more than one state transition as input. In this section, we aim to investigate how the length of the discriminator horizon may affect the learning process of the desired behaviors. Here we provide an evaluation in terms of the handcrafted reward of policies learned with discriminator observations of horizon  $H = 2, 4, 8$  with LSGAN and WASABI in SOLOSTANDUP. The result is depicted in Fig. S8.

Observe that a longer horizon tends to help the policy converge earlier and yield slightly better performance in terms of the handcrafted reward in both methods with either full or partial reference information, even if the LSGAN fails to learn the stand-up behavior. A similar pattern is also revealed in SOLOBACKFLIP, although it presents a weaker effect on policy convergence in comparison. The potential reason is that the policy learns to avoid producing state transitions that align with only a short sub-sequence of the reference motion. Such avoidance of mode collapse would prevent the policy from getting stuck at the local optima and thus increase the overall performance.

However, the benefit brought about by a longer discriminator observation horizon is not identified in tasks with hand-held reference motions where a direct performance metric is not applicable. Sometimes a longer horizon may even result in failure of learning the desired motion which is attainable with shorter horizons. An evaluation of performance improvement in terms of DTW over iterations reveals no clear pattern on how different discriminator observation horizons affect policy convergence. This may result from the time and state inconsistency in the hand-held reference motions which may already alleviate mode collapse to some extent.

## References

- [1] T. Giorgino. Computing and visualizing dynamic time warping alignments in r: the dtw package. *Journal of Statistical Software*, 31:1–24, 2009.
- [2] A. Mori, S. Uchida, R. Kurazume, R.-i. Taniguchi, T. Hasegawa, and H. Sakoe. Early recognition and prediction of gestures. In *18th International Conference on Pattern Recognition (ICPR'06)*, volume 3, pages 560–563. IEEE, 2006.